Published online 20 November 2009

Nucleic Acids Research, 2010, Vol. 38, No. 3 ***931–941***
doi:10.1093/nar/gkp1058

The helicase XPD unwinds bubble structures and is not stalled by DNA lesions removed by the nucleotide excision repair pathway

Jana Rudolf, Christophe Rouillon, Ulrich Schwarz-Linek and Malcolm F. White*

Centre for Biomolecular Sciences, University of St Andrews, St Andrews, Fife KY16 9ST, UK

Received June 19, 2009; Revised October 7, 2009; Accepted October 26, 2009

ABSTRACT

Xeroderma pigmentosum **factor D (XPD) is a 5′–3′ superfamily 2 helicase and the founding member of a family of DNA helicases with iron–sulphur cluster domains. As a component of transcription factor II H (TFIIH), XPD is involved in DNA unwinding during nucleotide excision repair (NER). Archaeal XPD is closely related in sequence to the eukaryal enzyme and the crystal structure of the archaeal enzyme has provided a molecular understanding of mutations causing xeroderma pigmentosum and trichothiodystrophy in humans. Consistent with a role in NER, we show that archaeal XPD can initiate unwinding from a DNA bubble structure, differentiating it from the related helicases FancJ and DinG. XPD was not stalled by substrates containing extrahelical fluorescein adducts, abasic sites nor a cyclobutane pyrimidine dimer, regardless of whether these modifications were placed on either the displaced or translocated strands. This suggests that DNA lesions repaired by NER may not present a barrier to XPD translocation *in vivo,* in contrast to some predictions. Preferential binding of a fluorescein-adducted oligonucleotide was observed, and XPD helicase activity was readily inhibited by both single- and double-stranded DNA binding proteins. These observations have several implications for the current understanding of the NER pathway.**

INTRODUCTION

Helicases are motor proteins, which use the free energy derived from NTP hydrolysis to translocate along nucleic acids. The hydrolysis of the β-γ phosphoanhydride bond promotes a molecular switch leading to conformational changes within the protein that result in translocation. This movement is used for the unwinding of nucleic acids or for the displacement of nucleic acid bound proteins. In 1993, Gorbalenya and Koonin (1) provided for the first time a method to categorize helicases on the basis of their conserved motifs. This led to the widely accepted classification of helicases into three superfamilies (SF1-3) and two smaller families (F4, F5). These (super)families are characterized by seven (SF1 and 2), three (SF3) and five (F4 and 5) conserved signature sequences, respectively, including the ubiquitous Walker A and B motifs. In the tertiary structure, helicase motifs cluster to form a cleft for nucleotide and nucleic acid binding situated between two motor domains that consist of RecA-type folds. Additional domains confer specificity for certain DNA or RNA structures or protein interaction partners and are thus specific for particular classes of helicases (2,3).

XPD (*Xeroderma pigmentosum* factor D) is a SF2 ATP-dependent 5′–3′ DNA helicase. In eukarya, XPD is part of a 10-subunit complex comprising the transcription factor II H (TFIIH) core complex and a cyclin-activating kinase (CAK) subcomplex (4–6). The TFIIH holocomplex is involved in transcription initiation of genes regulated by RNA polymerase II promoters. As part of the TFIIH core, the helicase activity of XPD is required in nucleotide excision repair (NER) but only its presence, not its activity, is required for transcription initiation (7,8). Mutations of

*To whom correspondence should be addressed. Tel: +44 1334 463432; Fax: +44 1334 462595; Email: mfw2@st-and.ac.uk
Present address:
Jana Rudolf, Wellcome Trust Centre for Molecular Parasitology and Division of Infection and Immunity, Faculty of Biomedical and Life Sciences, University of Glasgow, 120 University Place, Glasgow, G12 8TA, UK.

The authors wish it to be known that, in their opinion, the first two authors should be regarded as joint First Authors.

the xpd gene in humans can result in three distinct disorders: *Xeroderma pigmentosum* (XP), trichothiodystrophy (TTD) and Cockayne Syndrome (CS) combined with XP, depending on whether the helicase activity, interactions with TFIIH or both are affected (9,10).

Most archaeal genomes encode a clear homologue of XPD. Archaeal XPD is a monomer in solution and has no known stable interactions with other proteins, factors that have made it amenable to biochemical and structural studies. Characterization of archaeal XPD revealed the presence of a conserved iron–sulphur (Fe-S) cluster-binding domain that is essential for the helicase activity (11). The eukaryal XPD and related helicases FancJ, RTel1 and Chl1 are all predicted to have an Fe-S cluster binding domain, and a variety of mutations of XPD and FancJ in humans target this domain (11). Independently, three groups have recently solved structures of archaeal XPDs (12–14). All three structures revealed a four-domain organization, with the FeS cluster binding domain and an Arch domain arising from the first of two canonical helicase motor domains. The crystal structures of archaeal XPD allowed a molecular explanation for the consequences *in vivo* of many of the mutations seen in human xpd giving rise to XP, TTD and CS phenotypes.

In this study, we characterize the substrate specificity of archaeal XPD, showing that it can unwind a bubble substrate consistent with a role in NER. We show that the activity of XPD is readily inhibited by both single- and double-strand DNA binding proteins. Importantly, we demonstrate that XPD can unwind DNA containing the bulky extrahelical adduct fluorescein and a cyclopyrimidine dimer (CPD)—two examples of the types of lesion repaired by the NER pathway *in vivo*. These data suggest that models for damage detection by XPD stalling may require revision.

MATERIALS AND METHODS

Protein expression and purification

Wild-type XPD from *Sulfolobus acidocaldarius* was expressed and purified as described previously (11) with the exception that all purification buffers were first degassed with Argon gas to reduce the concentration of dissolved oxygen and protect the iron–sulphur cluster from oxidation. Alba1 and SSB from *S. solfataricus* were purified as described previously (15,16).

DNA substrates and helicase assays

DNA unwinding assays were performed essentially as described previously (13). Modifications to this method are indicated in the figure legends and Results section. Oligonucleotides were 5′-^{32}P-radiolabelled and annealed overnight by cooling from 90°C to room temperature. DNA substrates were gel purified and ethanol precipitated as described previously (17). The following oligonucleotides were purchased from Operon Biotechnologies GmbH, and annealed to make the substrates shown in Figure 1. CPD-containing oligonucleotides were purchased from Eurogentec.

45nt Fl	5′-CCGAATAGCGGAATTCACGAGTACCTGCGGCCTCGAGGGA[Fl∼dT]CCGT
45nt	5′-CCGAATAGCGGAATTCACGAGTACCTGCGGCCTCGAGGGATCCGT
60nt Fl	5′-CAGCGGCTTGCTAGTACGGA[Fl∼dT]CCCTCGAGGCCGCAGGTACTCGTGAATTCCGCTATTCGG
60nt	5′-CAGCGGCTTGCTAGTACGGATCCCTCGAGGCCGCAGGTACTCGTGAATTCCGCTATTCGG
45nt abasic	5′-CCGAATAGCGGAATTCACGAGTACCTGCGGCCTCGAGGGA[d-Sp]CCGT
60nt abasic	5′-CAGCGGCTTGCTAGTACGGA[dSp]CCCTCGAGGCCGCAGGTACTCGTGAATTCCGCTATTCGG
B25	5′-CCTCGAGGGATCCGTCCTAGCAAGC
B25comp	5′-GCTTGCTAGGACGGATCCCTCGAGG
B50	5′-CCTCGAGGGATCCGTCCTAGCAAGCCGCTGCTACCGGAAGCTTCTGGACC
H25	5′-GGTCCAGAAGCTTCCGGTAGCAGCG
H50	5′-GGTCCAGAAGCTTCCGGTAGCAGCGAGAGCGGTGGTTGAATTCCTCGACG
X50	5′-GCTCGAGTCTAGACTGCAGTTGAGAGCTTGCTAGGACGGATCCCTCGAGG
R25	5′-CGTCGAGGAATTCAACCACCGCTCT
R26-50	5′-TCTCAACTGCAGTCTAGACTCGAGC
R50	5′-CGTCGAGGAATTCAACCACCGCTCTTCTCAACTGCAGTCTAGACTCGAGC
Bubble 7	5′-GGTCCAGAAGCTTCCGGTAGCATACCGCAGCTAGGACGGATCCCTCGAGG
OhT6	5′-TTTTTTGCTTGCTAGGACGGATCCCTCGAGG
OhT9	5′-TTTTTTTTTGCTTGCTAGGACGGATCCCTCGAGG
OhT12	5′-TTTTTTTTTTTTGCTTGCTAGGACGGATCCCTCGAGG
OhT15	5′-TTTTTTTTTTTTTTTGCTTGCTAGGACGGATCCCTCGAGG
OhT20	5′-TTTTTTTTTTTTTTTTTTTTGCTTGCTAGGACGGATCCCTCGAGG
ITC-T8	5′-TTTTTTTT
ITC-T12	5′-TTTTTTTTTTTT
ITC-T16	5′-TTTTTTTTTTTTTTTT
ITC-T16F	5′-[Fl]TTTTTTTTTTTTTTTT
CPDcont	5′-CGATAAGCTTCTTCTTCTTTTCGGGTTTGGG
CPD	5′-CGATAAGCTTCTTCTTC[CPD]TTCGGGTTTGGG
CPDcomp31	5′-CCCAAACCCGAAAAGAAGAAGAAGCTTATCG
CPDcomp46	5′-TTTTTTTTTTTTTTTCCCAAACCCGAAAAGAAGAAGAAGCTTATCG
CPD AAcomp	5′-CCCAAACCCGAAAAGAAGA

For helicase assays carried out in the presence of Alba1 or SSB, the radiolabelled DNA substrate was incubated first with Alba1 or SSB for 1 min at room temperature, before XPD was added (200 nM unless stated otherwise). Reactions were incubated further for 1 min at 45°C, before initiation with a 1:1 mixture of $MgCl_2$:ATP (1 mM). Reactions were stopped at 3 min and samples separated on a 12% native acrylamide:TBE gel. Modifications from this method are indicated in the respective figure legends. The extent of DNA unwinding was quantified by phosphorimaging using a Fuji FLA5000 phosphorimager and Imagegauge software. The data were fitted using Equation 1, where k_1 = unwinding rate and k_2 = amplitude of unwinding.

$$\text{Fraction unwound} = k_2(1-\exp(-k_1 t)) \quad (1)$$

Name	Structure	Oligo-nucleo-tides
5' overhang	25 25	B25, X50
Splayed duplex		B50, X50
5' flap		B50, X50, H25
3' flap		B50, X50, R26-50
Nicked 3-way junction		B50, X50, H25, R26-50
Nicked 4-way junction		B50, X50, H50, R25, R26-50
7 nt bubble	7 21 22	B50, bubble 7
CPD control	31 15	CPDcont, CDPcomp 46
CPD displaced	12 31 15	CPD, CDPcomp 46
Duplex control	31	CPDcont, CPDcomp 31
CPD duplex	12 31	CPD, CPDcomp 31

Name	Structure	Oligonuc-leotides
T0		B25, B25comp
OhT6	6 nt dT	B25, OhT6
OhT9	9 nt dT	B25, OhT9
OhT12	12 nt dT	B25, OhT12
OhT15	15 nt dT	B25, OhT15
OhT20	20 nt dT	B25, OhT20
45/ 60 control	45 15	45nt, 60nt
Fl-1	4 45 15	45nt Fl, 60nt
Fl-2	4 45 15	45nt, 60nt Fl
Fl-3	4 45 15	45nt Fl, 60nt Fl
Ab-1	4 45 15	45nt abasic, 60nt
Ab-2	4 45 15	45nt, 60nt abasic
Ab-3	4 45 15	45nt abasic, 60nt abasic
CPD translc control	19 12	CPD_AA comp, CPDcont
CPD translc	19 12 17	CPD_AA comp, CPD

Figure 1. DNA constructs used in this study. Substrates were prepared by annealing the oligonucleotides indicated followed by purification from native polyacrylamide gels. The position of the 5′-^{32}P-label is indicated by a grey circle. The positions of modifications are indicated with symbols and discussed in the text.

Isothermal titration calorimetry

Isothermal titration calorimetry (ITC) experiments were carried out using a VP-ITC micro calorimeter (MicroCal^{TM}, Northampton, MA, USA). Protein was dialysed into ITC buffer (20 mM potassium phosphate, pH 7.8, 100 mM NaCl, 1 mM $MgCl_2$) overnight at 4°C. Oligonucleotides (ITC-T8, ITC-T12, ITC-T16 and ITC-T16 with a 5′-fluorescein; Operon Biotechnologies GmbH) were dissolved in ITC buffer and the pH of all

solutions measured and adjusted if necessary. Concentrations were determined using the absorbance at 280 and 260 nm, respectively, and the calculated extinction coefficients. All solutions were extensively degassed and reactions were carried out at 20°C. In a standard experiment, the cell contained 1.43 ml of a solution of 5 μM DNA oligomer and the syringe contained ~290 μl of XPD solution (148 μM for ITC-T8 and ITC-T12, 113 μM for ITC-T16 and ITC-T16F). Titrations were performed as follows: one preliminary injection of 2 μl was followed by 39 injections of 7 μl (ITC-T8 and ITC-T12) and 49 injections of 5 μl (ITC-T16 and ITC-T16Fl). The cell was stirred at 307 r.p.m.; the delay time between the injections was 3 min. To take into account heats of dilution, blank titrations were performed by injecting XPD solution into ITC buffer. Wherever possible these data were subtracted directly from the main experimental data. In case of constant (non-titrating) heats of dilution, a constant average value was subtracted. In case of small, noisy heats of dilution reflecting a titration, a linear regression of the heats of dilution was subtracted from the main experiment data. Data were analysed using MicroCal Origin software fitting them to a single binding site model. XPD concentrations were corrected to reflect 1:1 binding. All XPD solutions contained 70–75% effective (active) protein.

RESULTS

DNA substrate preference of XPD

It is necessary to delineate the structural requirements and the specificity of XPD with a variety of DNA substrates to understand the role of the archaeal enzyme *in vivo* and to inform our understanding of the eukaryal homologue during NER. Accordingly, we first analysed the minimal ssDNA binding site commensurate with XPD activity *in vitro*. The rate of DNA unwinding was measured using DNA substrates consisting of a 25 nt dsDNA region and different lengths of 5′-dT overhangs (0, 6, 9, 12, 15 and 20 T's, Figure 1). Rates from triplicate experiments were quantified using Equation 1 in 'Materials and Methods' section to yield unwinding rates and amplitudes (Figure 2). Substrates with overhangs of 0, 6 or 9 nt were unwound at similar rates and remained only partially unwound at the end of the reaction. Under different conditions, XPD is unable to unwind dsDNA molecules appreciably—see for example the data in Figure 6A. In contrast, overhangs of 12, 15 or 20 nt were unwound progressively more quickly and to completion. Similarly, human FancJ and *Escherichia coli* DinG did not show unwinding using a 10 nt 5′ overhang (18,19), whereas sufficient unwinding was observed with a 15 nt 5′ overhang, indicating that the ssDNA binding site of these enzymes is between 11 and 15 nt. The increase in unwinding rate observed as the overhang was increased from 12 to 15 and 20 nt is similar to the results reported for FancJ (19), and may reflect the assembly of more than one helicase enzyme on each substrate.

To examine the ssDNA binding affinity of XPD in solution, we used ITC and oligo-dT ligands of 8, 12 and

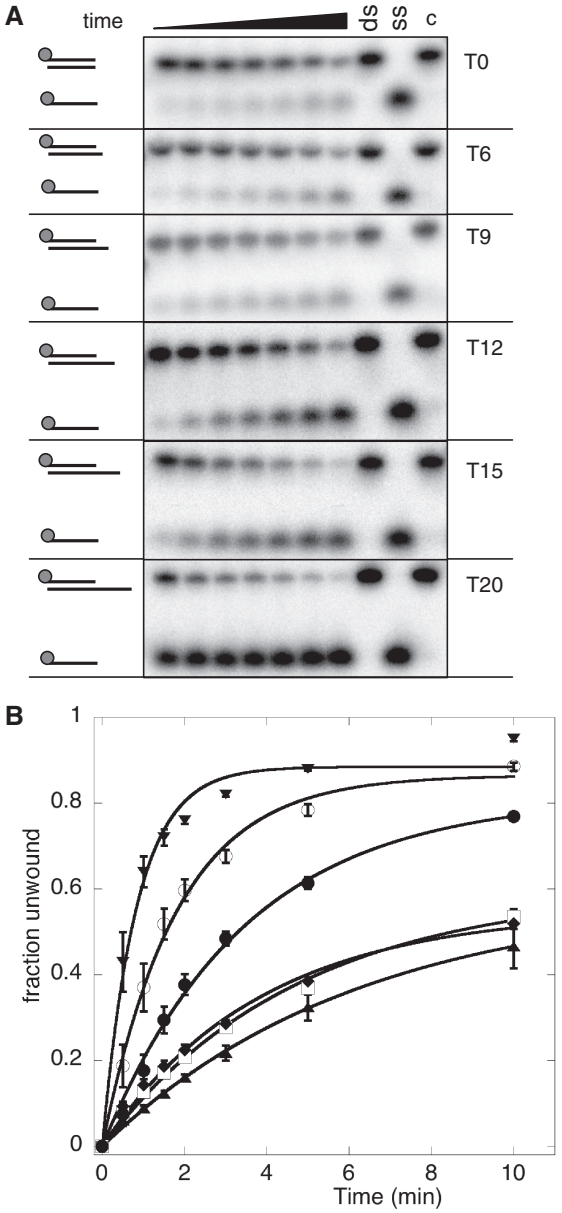

Figure 2. Substrate requirements of XPD. The DNA unwinding activity of XPD increases with increasing length of the 5′ ssDNA overhang. (**A**) Representative 12% acrylamide:TBE gels of XPD (200 nM) unwinding DNA providing 0, 6, 9, 12, 15 and 20 nt of 5′ ssDNA dT-overhangs (T0–T20) at 45°C. Time points were 0.5, 1, 1.5, 2, 3, 5 and 10 min. Controls: ss, boiled substrate; ds, intact substrate; C, substrate stability in the absence of XPD at the end point of the reaction. (**B**) The graph shows quantification of results of triplicate experiments with the standard errors indicated. The fraction of total DNA unwinding is plotted against the time and data points were fitted using equation 1. T0 (filled triangle); T6 (open square); T9 (filled diamond); T12 (filled circle); T15 (open circle) and T20 (inverted filled trianlge).

16 nt length (Figure 3). An 8 nt oligo (ITC-T8) was bound only very weakly by XPD, therefore it was not possible to determine the DNA binding affinity accurately, and the K_D was estimated to be in excess of 40 μM. A 12-mer (ITC-T12) was bound with a K_d of 5.6 μM, and a 16-mer (ITC-T16) bound more tightly with a K_d of

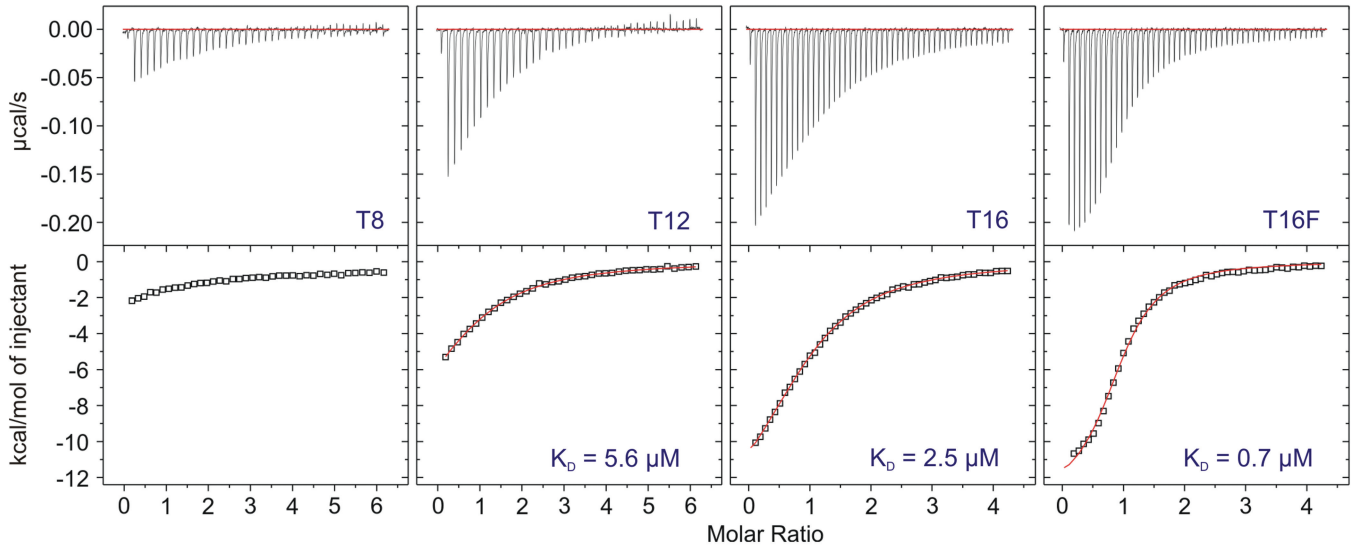

Figure 3. ITC analysis of DNA binding affinity. Isothermal titration calorimetry profiles for the interaction of XPD with oligonucleotides of different lengths. The top panel shows heat differences obtained for injections of 148 µM (ITC-T8 and ITC-T12) and 113 µM (ITC-T16 and ITC-T16F) XPD into 5 µM DNA solutions. The lower panel shows the incremental enthalpy changes, corrected for heats of dilution, with experimental points (open square) and the best fit (thin line). Data were fitted using a one-site binding model.

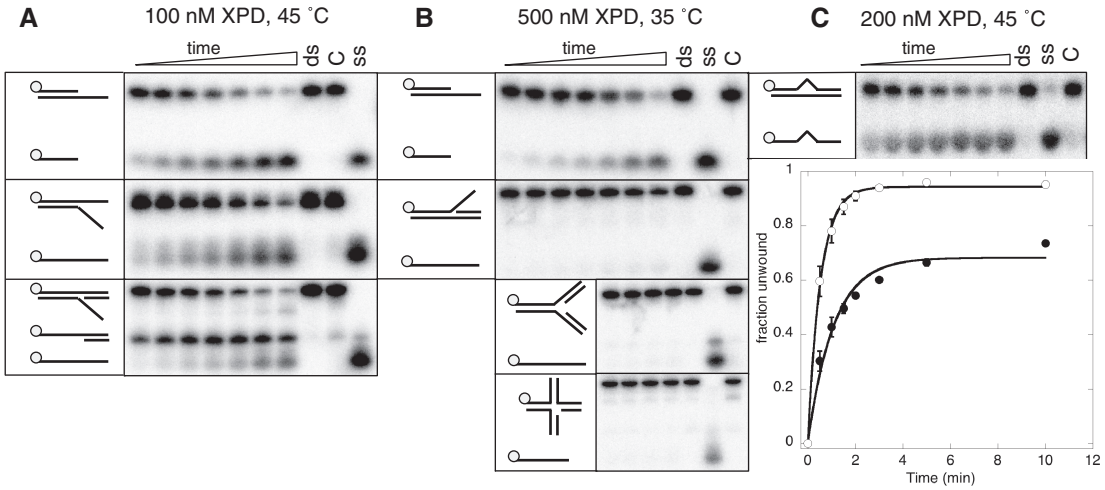

Figure 4. DNA substrate preference of XPD. The figure shows representative 12% acrylamide:TBE gels. The DNA structures before and after unwinding are shown to the left of the gels. Time points were 0.5, 1, 1.5, 2, 3, 5 and 10 min for all substrates except for the nicked three-way and four-way junctions (5, 10, 20 and 30 min). Controls: ss, boiled substrate; ds, intact substrate; C, substrate stability in the absence of XPD at the end point of the reaction. (**A**) XPD (100 nM) unwinding a 5′ overhang, splayed duplex and 5′ flap DNA substrate at 45°C. Reaction rates were all within a factor of 2. (**B**) XPD (500 nM) unwinding a 5′ overhang, a 3′ flap, a nicked three-way and a nicked four-way junction at 35°C. No significant unwinding was observed. (**C**) XPD (200 nM) unwinding a 7 nt bubble substrate at 45°C. The plot shows quantification of triplicate experiments with means and standard errors shown for the 7 nt bubble (filled circle) and a 25 nt overhang substrate (open circle).

2.5 µM. These data are consistent with those showing the length of ssDNA tail required for helicase activity. A 16-mer with an 5′-fluorescein adduct (ITC-T16F) was bound 3- to 4-fold more tightly than the corresponding unmodified oligonucleotide—an observation that will be discussed later.

We next investigated the specificity of XPD for different DNA structures using a variety of synthetic substrates depicted in Figure 1. The normal model substrate for XPD, a 5′ overhang, was unwound at similar rates (within 2-fold) as substrates with a 3′ ssDNA tail or a 3′ dsDNA tail (splayed duplex and 5′ flap DNA substrate) (Figure 4). In contrast, the two XPD homologues FancJ and DinG show appreciably more activity against splayed duplexes and 5′-flaps compared with simple overhangs (18,19). As expected, no activity was detected against a 3′ flap, a nicked three-way junction or a nicked four-way junction, indicating that a 5′ ssDNA stretch for loading of XPD is required.

The normal DNA substrate for eukaryal XPD does not have a free 5′- or 3′-end, and instead resembles a bubble structure that is enlarged by the action of XPD.

Accordingly, a DNA substrate containing a central 7 nt non-complementary region was tested. XPD unwound this substrate with a rate of 0.91 min^{-1}, compared to a rate of 1.9 min^{-1} for the standard 25 nt overhang substrate under the same conditions (Figure 4C). Indeed, the rate of unwinding of the 7 nt bubble structure was 3-fold faster than that observed with a 9 nt 5′ ssDNA overhang (Figure 2). This indicates that the presence of a free 5′ ssDNA end is not needed for the stimulation of the helicase activity. In contrast, the two related helicases FancJ and DinG are unable to unwind larger bubble structures (18,19). The ability of archaeal XPD to bind and unwind bubble structures is consistent with the role of the eukaryal protein *in vivo* and strengthens the hypothesis that archaeal XPD is also involved in NER.

XPD can overcome single backbone or base modifications in both the translocated and the displaced strand

A role for XPD in the detection of DNA damage during NER has been postulated, which requires physical stalling of the helicase at the lesion site (20). We used an internal fluorescein-dT moiety as an example of a bulky extrahelical modification that is repaired by the NER pathway. The modification site was located 5 nt from the ss/dsDNA junction within the duplex region. There was no discernible effect on helicase activity regardless of whether the modification was placed on the translocated strand, the displaced strand, or indeed on both simultaneously (Figure 5A). We repeated these experiments using a single 'dSpacer' abasic site analogue. Again, no discernible inhibition was observed when the abasic site was present in either strand or both simultaneously (Figure 5B). Since eukaryal XPD is involved in the NER pathway that removes UV photoproducts by unwinding around the lesion, we also tested the ability of XPD to unwind substrates containing a cyclobutane pyrimidine dimer (CPD) on either the displaced or translocated strands. As shown in Figure 5C, XPD unwound both substrates containing a CPD lesion at least as efficiently as the equivalent unmodified DNA. The substrate with the CPD in the translocated strand was assayed at 30°C as it was unstable at higher temperatures. This resulted in lower helicase activity against the unmodified control substrate, which can make two extra base pairs compared to the CPD-containing substrate (Figure 5C). While it is possible that XPD could stall at a lesion and still destabilize a small DNA duplex sufficiently to allow strand separation, this is not likely for the fluorescein-adducted substrates where the DNA duplex 3′ of the lesion was 40 bp in length. Altogether, these data suggest strongly that XPD can translocate past damaged DNA *in vitro*.

The influence of SSB on the activity of XPD

Single-stranded DNA binding proteins (SSB; Replication Protein A or RPA in eukarya) are found in all three domains of life, are abundant in the cell and play a role in every process that generates ssDNA, including DNA repair, replication and recombination. RPA is a key component of the eukaryal NER pathway; *S. solfataricus* SSB can also discriminate damaged and undamaged DNA and is therefore a potential candidate for DNA damage recognition in the archaeal NER pathway (21). Many SSBs have been demonstrated to interact physically and functionally with helicases, including RecQ (22), RecG (23), FancJ (24) and BLM (25), modulating their activity. The helicase activity of XPD from *Ferroplasma acidarmanus* is stimulated by the addition of a cognate RPA protein *in vitro* (26).

Therefore, we investigated to what extent *S. solfataricus* SSB influenced the helicase activity of XPD. The first substrate tested was a 31 bp blunt-ended DNA duplex containing a single CPD modification, and the corresponding unmodified duplex. SSB (500 nM) was added first and incubated with the DNA for 20 s before the addition of XPD (250 nM) and ATP. In the absence of SSB, XPD could not unwind either the unmodified or CPD-containing duplexes (Figure 6A). SSB on its own could melt the DNA duplex after incubation for 5 min, and was more efficient at melting the CPD-containing duplex than the unmodified one, as described previously (21). Surprisingly, when both proteins were together in the reaction, melting by SSB was decreased significantly (Figure 6A, lanes 5 and 6). This effect was independent of ATP and was observed for both the CPD-containing and control duplexes. One explanation is that XPD interacts with and stabilises the duplex DNA, preventing melting by SSB. To investigate the effect of SSB on the helicase activity of XPD, the same duplex DNA sequences were studied with the addition of a 5′ 15T tail to facilitate XPD loading. The helicase activity of XPD (250 nM) was inhibited significantly by the presence of an equimolar concentration of SSB (Figure 6B), presumably due to competition between the two proteins for binding to the ssDNA tail.

Experiments were then carried out at different molar ratios of XPD and SSB (Figure 6C). SSB began to inhibit the helicase activity of XPD (200 nM) at a sub-stoichiometric concentration (100 nM). At this concentration, minimal SSB-mediated DNA melting was observed, suggesting that SSB was bound on the ssDNA end. At 1 μM SSB, DNA melting was observed, with some protection apparent in the presence of XPD. The DNA duplex was melted completely by 10 μM SSB regardless of the presence or absence of XPD. These data suggest that crenarchaeal XPD and SSB influence one another's activity, but do not appear to cooperate in DNA damage detection and unwinding in this simplified *in vitro* system.

The influence of the dsDNA binding protein Alba1 on XPD helicase activity

Alba1 (Sso10b) is one of the main chromatin proteins present in *Sulfolobus* species and binds double-stranded DNA in a cooperative manner (15,27). Alba1 has been shown to protect dsDNA from melting by SSB (28) and incubation of a DNA substrate with 100 nM Alba1 resulted in complete inhibition of the replicative helicase MCM (50 nM) in *S. solfataricus* (29). We therefore investigated the effect of increasing concentrations of Alba1 on the helicase activity of XPD. A progressive inhibition of strand separation was observed, with complete

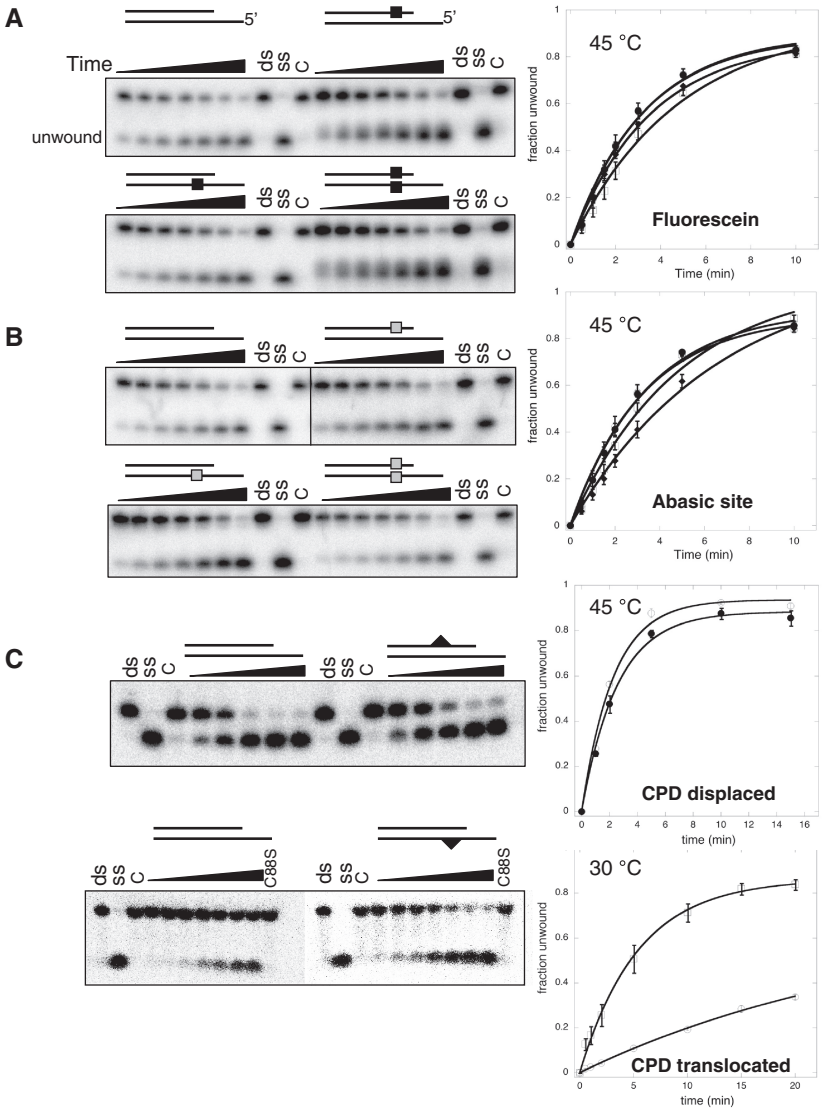

Figure 5. DNA modifications on the displaced or translocated strands do not affect the helicase activity of XPD. Representative 12% acrylamide:TBE gels are shown. Time points were 0.5, 1, 1.5, 2, 3, 5 and 10 min at 45°C for all experiments except those shown in the bottom panel where the CPD was in the translocating strand, where time points were 0.2, 1, 2, 5, 10, 15 and 20 min at 30°C. The DNA structures used are described in Figure 1. Filled squares represent the fluorescein backbone modification (**A**), open squares the position of the abasic site (**B**) and triangles the position of the CPD lesion (**C**). Controls were as follows: ss, boiled substrate; ds, intact substrate; C, substrate stability in the absence of ATP at the end point of the reaction; C88S, substrates incubated with an inactive mutant of XPD. The plots on the right show means and standard error bars for triplicate experiments, fitted using Equation 1, with the following symbols: (open circle), control, no modification; (filled circle), displaced strand; (open square), translocated strand; (filled diamond), both strands.

protection of dsDNA at an Alba1 concentration of 1 μM (Figure 6D). The same results were obtained using 600 nM XPD and it did not depend on in which order the proteins were added to the DNA prior to initiation of the unwinding reaction by addition of ATP (data not shown). In the cell, chromatin proteins are likely to prevent duplex DNA melting by SSB (28) and helicases will be required to remodel chromatin during DNA replication and repair.

DISCUSSION

Superfamily 1 and 2 helicases bind ssDNA or RNA across the top of the two canonical motor domains, a distance that is spanned by ~8 nt of nucleic acid (30–32). However, we have demonstrated that XPD binds an 8-mer oligonucleotide very weakly, and is not efficient in unwinding a DNA duplex from a 9 nt 5′ overhang. This probably reflects the requirement for the ssDNA end to pass between the Arch and FeS binding domains (Figure 7), beyond which the DNA duplex is separated by a mechanism that is as yet unknown. The two related helicases FancJ and DinG both exhibit SSB sites of 11-15 nt, showing that these properties are quite general for this class of helicases.

During NER, eukaryal XPD binds to a DNA:protein complex lacking any free DNA ends. Therefore, it follows that the closed interface between the Arch and FeS domains must open to allow the passage of one strand

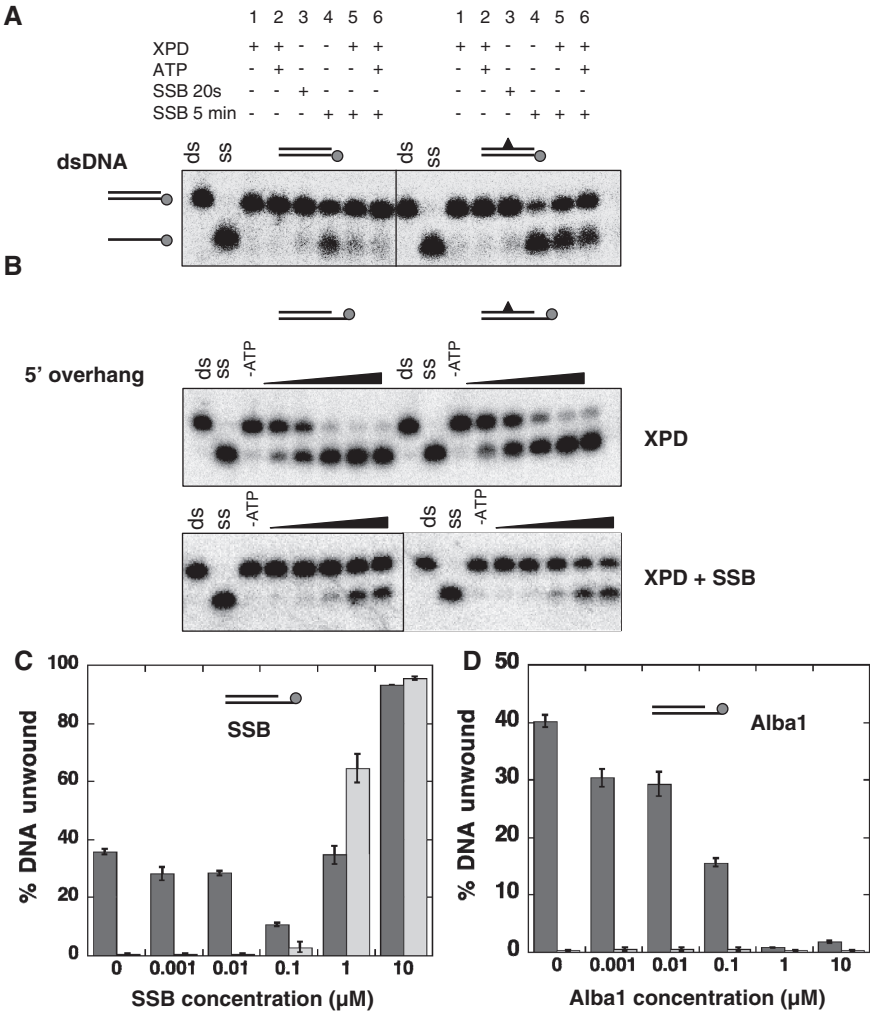

Figure 6. The influence of DNA binding proteins on the helicase activity of XPD. (**A**) DNA helicase assays were carried out using 10 nM of a 31 nt dsDNA substrate with or without a CPD lesion (Figure 1). The reactions were incubated at 45°C using the indicated combinations of 250 nM XPD, 500 nM SSB, 0.5 mM Mg-ATP. Controls are ds: DNA substrate; ss: boiled DNA. (**B**) Representative gels showing time courses of DNA unwinding reactions using a 31 nt duplex DNA substrate with or without a CPD lesion flanked by a 15 nt 5′overhang. Experiments were carried out with 250 nM XPD in the absence of SSB for 1, 2, 5, 10 and 15 min (top) or presence of 250 nM SSB for 0.5, 1, 2, 5 and 10 min (bottom). Controls are ds: DNA substrate; ss: boiled DNA; –ATP: substrate stability in the absence of ATP at the end point of the reaction. (**C**) The influence of increasing concentrations of SSB on the helicase activity of XPD is illustrated. The plot shows the mean values of duplicate experiments with the standard errors indicated. Experiments were carried out in the presence (dark grey bars) and absence (light grey bars) of 200 nM XPD at 45°C using the 45/60 control DNA substrate (10 nM, Figure 1) and increasing concentrations of SSB for 3 min. (**D**) The influence of increasing concentrations of Alba1 on the helicase activity of XPD is illustrated. For experimental conditions and analysis see above.

of ssDNA from the nascent DNA bubble formed around the lesion being repaired. Consistent with this, archaeal XPD has the ability to unwind bubble structures *in vitro*. The fact that XPD can unwind a 7 nt bubble more efficiently than a 9 nt 5′ overhang suggests that the former substrate is preferred. Possibly, favourable interactions with the displaced ssDNA strand of the bubble, and/or with the upstream or downstream DNA duplexes, help XPD to load at the bubble site and extend the region of unwound DNA. These data are thus consistent with the known role of eukaryal XPD and strengthen the hypothesis that archaeal XPD may also be involved in an excision DNA repair pathway. In contrast, DinG binds tightly to a DNA duplex containing an 11 nt bubble (K_d 100 nM) but cannot unwind it. DinG can however unwind D-loops (18). The role of DinG in bacteria is not yet clear as knockouts have only a very mild repair phenotype (33). The properties of FancJ *in vitro* also differentiate it from XPD. FancJ displayed no helicase activity against a substrate with a 21 nt DNA bubble (19) but unwinds D-loops, G4 quadruplexes (34,35) and DNA triplexes (36). FancJ is also sensitive to certain modified DNA structures, and is inhibited efficiently by a single thymine glycol in the translocating strand, although not by an 8-oxoguanine moiety (24).

In eukaryotic global genome NER, DNA damage can be recognised as a local distortion of the DNA double helix by the complex hr23B-XPC, which interacts with the non-damaged strand, opening up a small bubble of DNA around the lesion (37), (Figure 7A), allowing

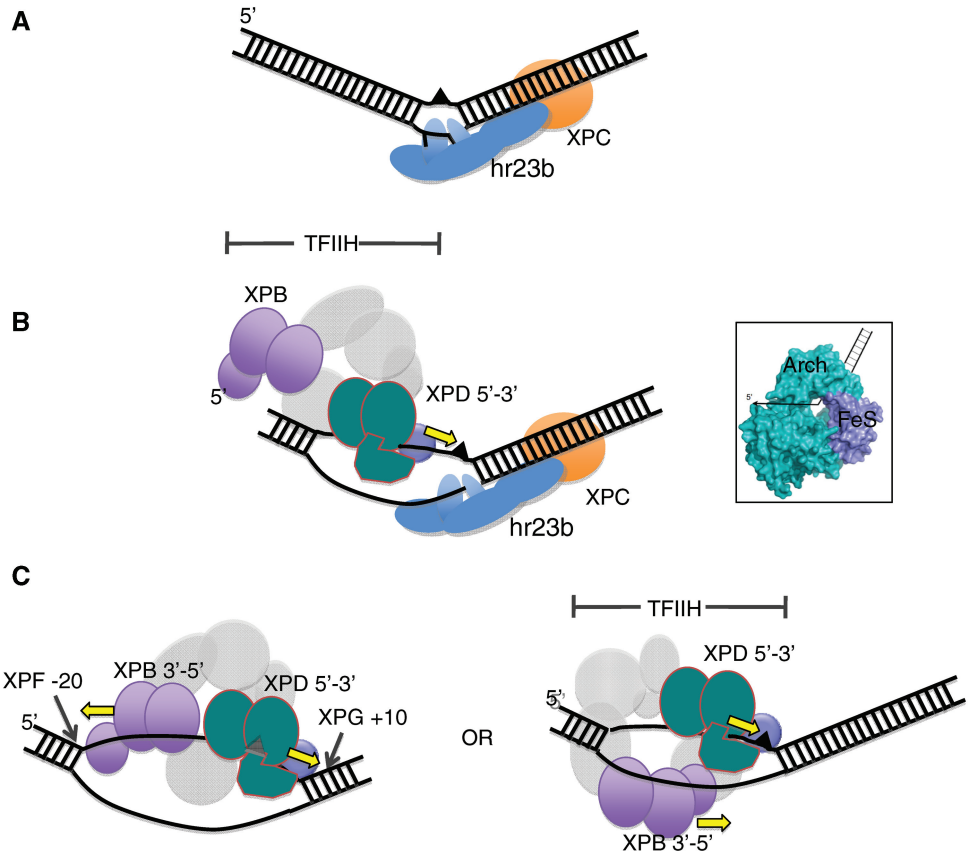

Figure 7. Model for the early steps in the eukaryal nucleotide excision repair pathway. (**A**) Initial damage recognition is carried out by hr23B-XPC, which binds the undamaged strand opposite a lesion as well as the duplex DNA downstream, opening a small ssDNA bubble. (**B**) Binding of TFIIH results in opening of at least 10 bp upstream (5′) of the damage site—enough to accommodate XPD on the damaged strand but not enough space to bind XPB simultaneously. XPD could extend the bubble by unwinding DNA in a 5′ to 3′ direction. The inset shows the structure of XPD from *Thermoplasma acidophilum* with the likely path of the DNA indicated. (**C**) Once the ssDNA bubble has been extended, XPB could bind at the 5′-end. The NER patch size is likely to be defined by the length of DNA bound by the combined actions of XPD and XPB. XPD can unwind DNA past the lesion but could be stalled by collision with hr23B-XPC and/or by constraints imposed by the rest of the TFIIH complex including XPB. In subsequent steps XPA and RPA replace the hr23B-XPC complex, and cleavage is catalysed by XPG and XPF-ERCC1. Alternatively, XPB could bind on the undamaged strand. Both helicases would then migrate in the same direction, tracking on separate strands.

recruitment of TFIIH. TFIIH binding initially results in a ssDNA bubble of around 10 nt upstream of the lesion, as judged by permanganate probing (8). This length of ssDNA suggests that only one of the TFIIH helicases binds initially, and extends the ssDNA bubble until the second can also bind. It is possible that XPD binds first, upstream of the damage, and moves in a 5′ to 3′ direction on the damaged strand (Figure 7B), consistent with the ability of archaeal XPD to bind to a small bubble substrate. Considering the known ssDNA binding site size of helicases such as XPB and XPD, the total length of ssDNA bound by these enzymes is likely to be at least 25 nt in length. If both helicases bind to the damaged strand as shown in Figure 7C then it seems likely that together they are responsible for defining the size of the patch of damaged DNA that is removed by the NER pathway—a point that is often not appreciated when considering models of NER. XPB has the opposite polarity to XPD and may be not so much a helicase as an ATP dependent conformational switch (8,38). In this scenario, XPB could define the upstream end of the NER complex at the junction between ssDNA and dsDNA 5′ of the lesion. The alternative possibility is that XPB might bind to the undamaged strand. Both helicases could then move in the same direction on opposing strands, towards the bound hr23B-XPC complex downstream of the lesion (Figure 7C, right panel). Currently, the data from studies of eukaryal NER does not explicitly rule out either possibility, although a recent paper from Coin and colleagues reports that the ATPase activity of XPB, but not XPD, is required for recruitment of TFIIH to DNA damage sites (39).

It has been suggested that XPD might, like the bacterial NER helicase UvrB, act as the damage sensor, binding the damaged strand 5′ of the lesion, translocating towards the lesion and stalling there, allowing recruitment and assembly of the other NER factors (20). This hypothesis has arisen in part from very early studies of recombinant *S. cerevisiae* Rad3 that suggested the helicase activity of Rad3 was inhibited by UV- and cisplatin-mediated DNA damage, particularly in the translocating strand (40,41). There are however some reasons to be cautious when

interpreting these observations. First, UV radiation of DNA results in a spectrum of damage types including strand breaks and oxidative effects in addition to the generation of photoproducts. Second, Rad3 was assayed in the absence of the other subunits of TFIIH that are now known to be essential for its full activity. The same set of experiments showed that Rad3 was also inhibited by the presence of abasic sites, which are not NER substrates *in vitro* (42).

Here, we have shown that XPD helicase activity is remarkably insensitive to the presence of DNA modifications, displaying efficient unwinding of DNA containing abasic sites, bulky extrahelical fluorescein adducts or a CPD. Given that the nucleases XPF-ERCC1 and XPG cleave the DNA at around positions −20 5′ to the lesion and +10 3′ to the lesion, respectively (43), and the likelihood that at least 25 nt of ssDNA are bound by XPD and XPB, it follows that XPD must be able to accept bulky DNA lesions through the choke point formed by the Arch and FeS cluster domains where the DNA duplex is broken. This is consistent with our observation that XPD can unwind DNA containing such lesions in the translocated strand. Single molecule studies of XPD have suggested that the archaeal enzyme may even be able to bypass bound SSB proteins during translocation (44). In eukarya, the NER bubble has been shown to extend 5 nt past a cisplatin adduct on the 3′ side, suggesting that unwinding can continue past a lesion (45). The translocation of XPD may stop once XPB is established at the other end of the NER bubble, since the two enzymes are linked physically. Alternatively, XPD may collide with the hr23B-XPC complex on the 3′ side of the lesion—the archaeal enzyme is certainly quite sensitive to the presence of bound proteins *in vitro*.

In either event, the final position of XPD in the NER complex is likely to position the lesion close to the XPD protein. The ITC data presented in Figure 3 raise the tantalizing prospect that XPD has a preference for binding DNA containing at least one type of NER lesion, as a 16dT oligonucleotide containing a fluorescein adduct was bound 3- to 4-fold more tightly by XPD than the unmodified oligonucleotide. As Figure 7B shows, it is likely that XPD is oriented such that the FeS cluster domain is positioned close to the DNA lesion. The presence of an iron–sulphur cluster in XPD at a position in close proximity to the path of the DNA has prompted suggestions that the cluster is used as a redox-active DNA damage sensor (11,12). Potentially, electron transfer from the cluster to the DNA could be used to detect DNA damage during the NER process, akin to the role proposed for FeS clusters in glycosylases (46). The alternative to this attractive hypothesis is the possibility that the FeS clusters in the XPD family helicases have a purely structural role, and it has been pointed out that the four human XPD-family helicases are not all likely to be involved in DNA damage detection but rather need the FeS binding domain for DNA strand separation (47). Nevertheless, given that XPD is probably the founding helicase of this family it is plausible that a damage-sensing role for the FeS cluster is the original function, even if it is no longer required by the other helicases. Another alternative is that FeS clusters provide a means to control the activities of DNA replication and repair proteins in response to redox stress or other signals in the cell. The FeS cluster in *E. coli* DinG has been shown to be redox-active but insensitive to high concentrations of the oxidizing agent hydrogen peroxide (48). However, the FeS cluster can be modified by nitrous oxide (NO), inactivating the helicase, raising the exciting possibility that NO could influence the activity of a variety of FeS containing proteins in human health and disease (48).

ACKNOWLEDGEMENTS

Thanks to Catherine Botting and the Mass spectrometry unit at St Andrews, which is funded by the Wellcome Trust, and to Paul Talbot for technical support. Thanks to Stuart MacNeill and Anne-Marie McRobbie for helpful discussions.

FUNDING

Funding for open access charge: Cancer Research UK, C22223 (Grant no. C22223 to M.F.W.). Funding for open access charge: University of St Andrews, UK.

Conflict of interest statement. None declared.

REFERENCES

1. Gorbalenya,A.E. and Koonin,E.V. (1993) Helicases: amino acid sequence comparisons and structure-function relationships. *Curr. Opin. Struct. Biol.*, **3**, 419–429.
2. Singleton,M.R., Dillingham,M.S. and Wigley,D.B. (2007) Structure and mechanism of helicases and nucleic acid translocases. *Annu. Rev. Biochem.*, **76**, 23–50.
3. Singleton,M.R. and Wigley,D.B. (2002) Modularity and specialization in superfamily 1 and 2 helicases. *J. Bacteriol.*, **184**, 1819–1826.
4. Schaeffer,L., Roy,R., Humbert,S., Moncollin,V., Vermeulen,W., Hoeijmakers,J.H., Chambon,P. and Egly,J.M. (1993) DNA repair helicase: a component of BTF2 (TFIIH) basic transcription factor. *Science*, **260**, 58–63.
5. Feaver,W.J., Svejstrup,J.Q., Bardwell,L., Bardwell,A.J., Buratowski,S., Gulyas,K.D., Donahue,T.F., Friedberg,E.C. and Kornberg,R.D. (1993) Dual roles of a multiprotein complex from S. cerevisiae in transcription and DNA repair. *Cell*, **75**, 1379–1387.
6. Giglia-Mari,G., Coin,F., Ranish,J.A., Hoogstraten,D., Theil,A., Wijgers,N., Jaspers,N.G., Raams,A., Argentini,M., van der Spek,P.J. *et al.* (2004) A new, tenth subunit of TFIIH is responsible for the DNA repair syndrome trichothiodystrophy group A. *Nat. Genet.*, **36**, 714–719.
7. Winkler,G.S., Araujo,S.J., Fiedler,U., Vermeulen,W., Coin,F., Egly,J.M., Hoeijmakers,J.H., Wood,R.D., Timmers,H.T. and Weeda,G. (2000) TFIIH with inactive XPD helicase functions in transcription initiation but is defective in DNA repair. *J. Biol. Chem.*, **275**, 4258–4266.
8. Coin,F., Oksenych,V. and Egly,J.M. (2007) Distinct roles for the XPB/p52 and XPD/p44 subcomplexes of TFIIH in damaged DNA opening during nucleotide excision repair. *Mol. Cell*, **26**, 245–256.
9. Lehmann,A.R. (2003) DNA repair-deficient diseases, xeroderma pigmentosum, Cockayne syndrome and trichothiodystrophy. *Biochimie*, **85**, 1101–1111.
10. Lehmann,A.R. (2008) XPD structure reveals its secrets. *DNA Repair.*, **7**, 1912–1915.
11. Rudolf,J., Makrantoni,V., Ingledew,W.J., Stark,M.J. and White,M.F. (2006) The DNA repair helicases XPD and FancJ have essential iron-sulfur domains. *Mol. Cell*, **23**, 801–808.

12. Fan,L., Fuss,J.O., Cheng,Q.J., Arvai,A.S., Hammel,M., Roberts,V.A., Cooper,P.K. and Tainer,J.A. (2008) XPD helicase structures and activities: insights into the cancer and aging phenotypes from XPD mutations. *Cell*, **133**, 789–800.
13. Liu,H., Rudolf,J., Johnson,K.A., McMahon,S.A., Oke,M., Carter,L., McRobbie,A.M., Brown,S.E., Naismith,J.H. and White,M.F. (2008) Structure of the DNA repair helicase XPD. *Cell*, **133**, 801–812.
14. Wolski,S.C., Kuper,J., Hanzelmann,P., Truglio,J.J., Croteau,D.L., Van Houten,B. and Kisker,C. (2008) Crystal structure of the FeS cluster-containing nucleotide excision repair helicase XPD. *PLoS Biol.*, **6**, e149.
15. Jelinska,C., Conroy,M.J., Craven,C.J., Hounslow,A.M., Bullough,P.A., Waltho,J.P., Taylor,G.L. and White,M.F. (2005) Obligate heterodimerization of the archaeal Alba2 protein with Alba1 provides a mechanism for control of DNA packaging. *Structure*, **13**, 963–971.
16. Wadsworth,R.I. and White,M.F. (2001) Identification and properties of the crenarchaeal single-stranded DNA binding protein from *Sulfolobus solfataricus*. *Nucleic Acids Res.*, **29**, 914–920.
17. Kvaratskhelia,M. and White,M.F. (2000) An archaeal Holliday junction resolving enzyme with unique properties. *J. Mol. Biol.*, **295**, 193–202.
18. Voloshin,O.N. and Camerini-Otero,R.D. (2007) The DinG protein from Escherichia coli is a structure-specific helicase. *J. Biol. Chem.*, **282**, 18437–18447.
19. Gupta,R., Sharma,S., Sommers,J.A., Jin,Z., Cantor,S.B. and Brosh,R.M. Jr (2005) Analysis of the DNA substrate specificity of the human BACH1 helicase associated with breast cancer. *J. Biol. Chem.*, **280**, 25450–25460.
20. Scharer,O.D. (2007) Achieving broad substrate specificity in damage recognition by binding accessible nondamaged DNA. *Mol. Cell*, **28**, 184–186.
21. Cubeddu,L. and White,M.F. (2005) DNA damage detection by an archaeal single-stranded DNA-binding protein. *J. Mol. Biol.*, **353**, 507–516.
22. Shereda,R.D., Bernstein,D.A. and Keck,J.L. (2007) A central role for SSB in Escherichia coli RecQ DNA helicase function. *J. Biol. Chem.*, **282**, 19247–19258.
23. Buss,J.A., Kimura,Y. and Bianco,P.R. (2008) RecG interacts directly with SSB: implications for stalled replication fork regression. *Nucleic Acids Res.*, **36**, 7029–7042.
24. Suhasini,A.N., Sommers,J.A., Mason,A.C., Voloshin,O.N., Camerini-Otero,R.D., Wold,M.S. and Brosh,R.M. Jr. (2009) FANCJ helicase uniquely senses oxidative base damage in either strand of duplex DNA and is stimulated by RPA to unwind the damaged DNA substrate in a strand-specific manner. *J. Biol. Chem.*, **284**, 18458–18470.
25. Brosh,R.M. Jr, Li,J.L., Kenny,M.K., Karow,J.K., Cooper,M.P., Kureekattil,R.P., Hickson,I.D. and Bohr,V.A. (2000) Replication protein A physically interacts with the Bloom's syndrome protein and stimulates its helicase activity. *J. Biol. Chem.*, **275**, 23500–23508.
26. Pugh,R.A., Lin,Y., Eller,C., Leesley,H., Cann,I.K. and Spies,M. (2008) Ferroplasma acidarmanus RPA2 facilitates efficient unwinding of forked DNA substrates by monomers of FacXPD helicase. *J. Mol. Biol.*, **383**, 982–998.
27. Bell,S.D., Botting,C.H., Wardleworth,B.N., Jackson,S.P. and White,M.F. (2002) The interaction of Alba, a conserved archaeal chromatin protein, with Sir2 and its regulation by acetylation. *Science*, **296**, 148–151.
28. Richard,D.J., Bell,S.D. and White,M.F. (2004) Physical and functional interaction of the archaeal single-stranded DNA binding protein SSB with RNA polymerase. *Nucleic Acids Res.*, **32**, 1065–1074.
29. Marsh,V.L., McGeoch,A.T. and Bell,S.D. (2006) Influence of chromatin and single strand binding proteins on the activity of an archaeal MCM. *J. Mol. Biol.*, **357**, 1345–1350.
30. Kim,J.L., Morgenstern,K.A., Griffith,J.P., Dwyer,M.D., Thomson,J.A., Murcko,M.A., Lin,C. and Caron,P.R. (1998) Hepatitis C virus NS3 RNA helicase domain with a bound oligonucleotide: the crystal structure provides insights into the mode of unwinding. *Structure*, **6**, 89–100.
31. Buttner,K., Nehring,S. and Hopfner,K.P. (2007) Structural basis for DNA duplex separation by a superfamily-2 helicase. *Nat. Struct. Mol. Biol.*, **14**, 647–652.
32. Velankar,S.S., Soultanas,P., Dillingham,M.S., Subramanya,H.S. and Wigley,D.B. (1999) Crystal structures of complexes of PcrA DNA helicase with a DNA substrate indicate an inchworm mechanism. *Cell*, **97**, 75–84.
33. Voloshin,O.N., Vanevski,F., Khil,P.P. and Camerini-Otero,R.D. (2003) Characterization of the DNA damage-inducible helicase DinG from Escherichia coli. *J. Biol. Chem.*, **278**, 28284–28293.
34. London,T.B., Barber,L.J., Mosedale,G., Kelly,G.P., Balasubramanian,S., Hickson,I.D., Boulton,S.J. and Hiom,K. (2008) FANCJ Is a Structure-specific DNA helicase associated with the maintenance of genomic G/C tracts. *J. Biol. Chem.*, **283**, 36132–36139.
35. Wu,Y., Shin-ya,K. and Brosh,R.M. Jr (2008) FANCJ helicase defective in Fanconia anemia and breast cancer unwinds G-quadruplex DNA to defend genomic stability. *Mol. Cell Biol.*, **28**, 4116–4128.
36. Sommers,J.A., Rawtani,N., Gupta,R., Bugreev,D.V., Mazin,A.V., Cantor,S.B. and Brosh,R.M. Jr. (2009) FANCJ uses its motor ATPase to destabilize protein-DNA complexes, unwind triplexes, and inhibit RAD51 strand exchange. *J. Biol. Chem.*, **284**, 7505–7517.
37. Min,J.H. and Pavletich,N.P. (2007) Recognition of DNA damage by the Rad4 nucleotide excision repair protein. *Nature*, **449**, 570–575.
38. Richards,J.D., Cubeddu,L., Roberts,J., Liu,H. and White,M.F. (2008) The archaeal XPB protein is a ssDNA-dependent ATPase with a novel partner. *J. Mol. Biol.*, **376**, 634–644.
39. Oksenych,V., de Jesus,B.B., Zhovmer,A., Egly,J.M. and Coin,F. (2009) Molecular insights into the recruitment of TFIIH to sites of DNA damage. *EMBO J.*, **28**, 2971–2980.
40. Naegeli,H., Bardwell,L. and Friedberg,E.C. (1992) The DNA helicase and adenosine triphosphatase activities of yeast Rad3 protein are inhibited by DNA damage. A potential mechanism for damage-specific recognition. *J. Biol. Chem.*, **267**, 392–398.
41. Naegeli,H., Modrich,P. and Friedberg,E.C. (1993) The DNA helicase activities of Rad3 protein of Saccharomyces cerevisiae and helicase II of Escherichia coli are differentially inhibited by covalent and noncovalent DNA modifications. *J. Biol. Chem.*, **268**, 10386–10392.
42. Naegeli,H., Bardwell,L. and Friedberg,E.C. (1993) Inhibition of Rad3 DNA helicase activity by DNA adducts and abasic sites: implications for the role of a DNA helicase in damage-specific incision of DNA. *Biochemistry*, **32**, 613–621.
43. Tapias,A., Auriol,J., Forget,D., Enzlin,J.H., Scharer,O.D., Coin,F., Coulombe,B. and Egly,J.M. (2004) Ordered conformational changes in damaged DNA induced by nucleotide excision repair factors. *J. Biol. Chem.*, **279**, 19074–19083.
44. Honda,M., Park,J., Pugh,R.A., Ha,T. and Spies,M. (2009) Single-molecule analysis reveals differential effect of ssDNA-binding proteins on DNA translocation by XPD helicase. *Mol. Cell*, **35**, 694–703.
45. Evans,E., Moggs,J.G., Hwang,J.R., Egly,J.M. and Wood,R.D. (1997) Mechanism of open complex and dual incision formation by human nucleotide excision repair factors. *EMBO J.*, **16**, 6559–6573.
46. Boal,A.K., Yavin,E., Lukianova,O.A., O'Shea,V.L., David,S.S. and Barton,J.K. (2005) DNA-bound redox activity of DNA repair glycosylases containing [4Fe-4S] clusters. *Biochemistry*, **44**, 8397–8407.
47. White,M.F. (2009) Structure, function and evolution of the XPD family of iron-sulfur-containing 5′→3′ DNA helicases. *Biochem. Soc. Trans.*, **37**, 547–551.
48. Ren,B., Duan,X. and Ding,H. (2009) Redox control of the DNA damage-inducible protein DinG helicase activity via its iron-sulfur cluster. *J. Biol. Chem.*, **284**, 4829–4835.